

Capabilities of LEWICE 1.6 and Comparison with Experimental Data

William B. Wright
NYMA, Inc.
Brook Park, OH

Abstract

A research project is underway at NASA Lewis to produce a computer code which can accurately predict ice growth under any meteorological conditions for any aircraft surface. The most recent release of this code is LEWICE 1.6. This paper will demonstrate some of the newer capabilities of this code as well as describe each of these advancements in full and make comparisons with the experimental data available. Further refinement of these features and inclusion of additional features continue to be performed on this model.

Nomenclature

A	Area (m ²)
a _p	Particle acceleration (m/s ²)
C _d	Drag coefficient
C _l	Lift coefficient
C _m	Moment coefficient
d	particle diameter (microns)
D	Drag force (N)
g	gravity (m/s ²)
L	Lift force (N)
m	mass (kg)
M	Moment force (N)
Oh	Ohnesorge number
Re	Reynolds number
V	velocity (m/s)
We	Weber number
x	x-coordinate (m)
\dot{x}	particle velocity in x (m/s)
\ddot{x}	particle acceleration in x (m/s ²)
y	y-coordinate (m)
\dot{y}	particle velocity in y (m/s)
\ddot{y}	particle acceleration in y (m/s ²)

α	angle of attack (deg)
γ	angle of particle to flow
μ	viscosity (kg/m s)
ν	kinematic viscosity (m ² /s)
θ	pitch angle (deg)
$\ddot{\theta}$	second derivative of pitch angle with time
ρ	density (kg/m ³)

Subscripts

a	air
p	particle
x	x-direction
y	y-direction

Introduction

The Icing Branch at NASA Lewis has undertaken a research project to produce a computer code capable of accurately predicting ice growth under any meteorological conditions for any aircraft surface. The most recent release of this code is LEWICE 1.6 which has now been documented in several reports^{1,2,3}. This paper will not go into the details of the improvements as those features are well-described by the previous reports. This paper will demonstrate some of the newer capabilities with a number of example cases supported by experimental data.

First, a theoretical evaluation is performed to ascertain the capabilities of LEWICE 1.6 for large drops. Then a parameter study is performed to show typical results in this regime. An MS-317 airfoil was selected for these runs as this model could be put in the IRT at a later date to verify these results. A range of drop sizes from 10 micron to 1000 micron was selected. These limits were chosen so as to fill out a log scale plot. Local and total collection efficiencies,

impingement limits, and maximum local collection efficiency are presented.

Second, the multi-body capability is shown by performing several comparisons with experimental data obtained in the NASA Lewis IRT. The case presented in this paper is for a McDonnell-Douglas 3-element airfoil. Ice shapes for this model were obtained in the IRT. The results of this test are presented at this conference⁴. Third, several predictions are made on a Learjet GLC305 airfoil for which experimental data has not yet been obtained. This represents the first known paper to present a 'blind' prediction so that an objective evaluation can be made of its capabilities. In all previous comparisons, code predictions are made after the ice shapes have been created. Then, by adjusting code parameters such as 'sand-grain' roughness, the best predictions are published. As LEWICE 1.6 uses a theoretical model to predict 'sand-grain' roughness, there is no possibility of altering the final predictions. Therefore, the predictions are made prior to the IRT test. The Learjet airfoil is the first of several IRT entries designed to produce a database of ice shapes for modern airfoils.

Drop Size Study

Droplet Trajectory Theory

This section will present the assumptions used in the droplet trajectory code in LEWICE 1.6 and evaluate their applicability for large drops. A large drop in this context applies to any drop size larger than 40 μm , the current upper limit in the FAA certification envelope. LEWICE 1.6 currently uses the following assumptions:

- solid particles
- spherical particles
- drops do not breakup due to acceleration
- particles do not rotate
- particles have no lift
- particles have no moment
- drag for a stationary sphere applies
- no transient effects due to changing drag
- evaporation of the drop is negligible
- turbulence effects are neglected
- flow is incompressible
- drops do not interact with each other
- continuum flow around drop
- all drops which strike the airfoil impinge

The equations of motion of an arbitrarily shaped particle are derived from a force balance on a point mass⁵:

$$m\ddot{x} = -\vec{D}\cos\gamma - \vec{L}\sin\gamma + mg\sin\alpha$$

$$m\ddot{y} = -\vec{D}\sin\gamma + \vec{L}\cos\gamma - mg\cos\alpha$$

where

$$\gamma = \text{atan}\frac{\dot{y}_p - V_y}{\dot{x}_p - V_x}$$

For an airfoil at an angle of attack α , the coordinate system is at an angle to the gravitational coordinate system. Therefore, the effect of gravity must be accounted for in the equations for both lift and drag.

The flow field velocity components in the x and y directions, i.e., V_x and V_y , respectively, are obtained from the potential flow program. The aerodynamic drag and lift forces are defined as

$$\vec{D} = c_d \frac{\rho_a V^2}{2} A_p$$

$$\vec{L} = c_l \frac{\rho_a V^2}{2} A_p$$

where A_p is a characteristic area of the particle, ρ_a is the density of air at the position of the particle, and V_R is the particle velocity relative to the flow field and defined as

$$V_R = \sqrt{(\dot{x}_p - V_x)^2 + (\dot{y}_p - V_y)^2}$$

For arbitrarily shaped particles, the pitch angle, θ_p , is required to evaluate the angle of attack α_p , using the following equation

$$\alpha_p = \theta_p - \gamma$$

This motion is governed by the following equation

$$\ddot{\theta} = \frac{M}{I_{zz}}$$

where I_{zz} , is the moment of inertia of mass relative to the z axis. The moment of aerodynamic forces acting on the particle is

$$M = c_m \frac{\rho_a V^2}{2} A_p d_p$$

where c_m is the pitching moment coefficient which must also be specified by the user.

The lift, drag, and pitching moment coefficients, c_l , c_d , and c_m respectively, must be provided by the user for arbitrarily shaped particles. The coefficient data should be functions of the particle angle of attack and the particle Reynolds number based on the particle diameter, given by the following equation:

$$Re_p = \frac{V d_p}{\nu}$$

The diameter of the particle, d , and the kinematic viscosity of air, ν , are assumed constant along the trajectory of the particle.

Since water droplets are usually assumed to be rigid spheres in icing studies, the only forces considered to be acting on the particle are those of drag and gravity. The governing equations can therefore be simplified as follows:

$$m\ddot{x} = -\vec{D}\cos\gamma + mg\sin\alpha$$

$$m\ddot{y} = -\vec{D}\sin\gamma - mg\cos\alpha$$

In this case, the drag force is determined using a steady-state drag coefficient for a sphere which is a function of the droplet Reynolds number, Re_p .

A complete evaluation of all the above assumptions has not been performed. The assumptions which have been evaluated are those which are believed to have the strongest effect on the governing equations. The evaluation uses drop sizes up to 1000 microns which represents the largest drop size ran so far with LEWICE 1.6. The reference used for this evaluation was Clift, Grace and Weber⁵ unless otherwise noted.

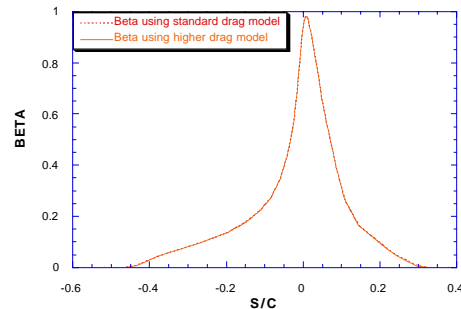
Spherical Particles

This assumption states that the drop remains spherical and does not deform due to the drop velocity. Beard and Pruppacher⁶ measured large drops falling in air due to gravity and showed that this effect can be taken into effect by using an alternate drag model, which at most is 15% higher than the drag on a sphere. In addition, negligible effect on lift and moment were seen. A test case was then constructed using an MS-317 airfoil. The following conditions were used:

$$\begin{aligned} \alpha &= 2^\circ \\ LWC &= 0.34 \text{ g/m}^3 \\ V &= 195 \text{ mph} \\ T &= -10^\circ \text{C} \\ MVD &= 1000 \text{ } \mu\text{m} \end{aligned}$$

The first case uses the standard drag model used in LEWICE 1.6. The second case then increased this value 15% for the entire Reynolds number range. This is a more severe requirement than the Beard and Pruppacher model where the drag at low Reynolds numbers conforms to the standard model. The collection efficiencies for these two cases are shown in Figure 1. As can be seen from this figure, the effect of drop deformation on collection efficiency is negligible.

FIGURE 1. Drag effect of non-spherical drop



Drop Breakup

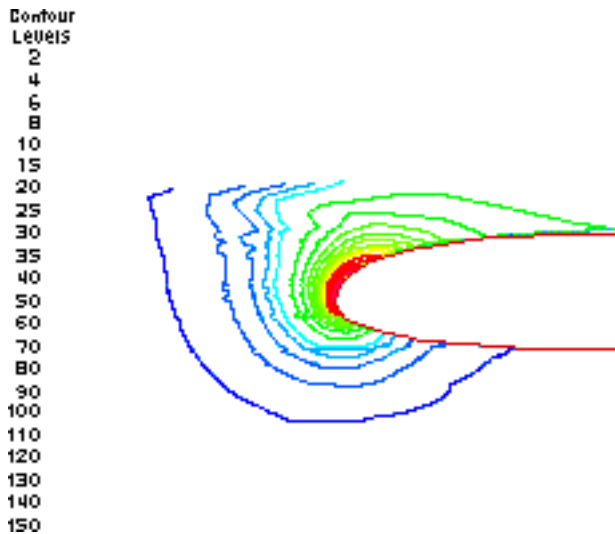
If a large drop moves at a high enough velocity, it can breakup due to shear. Breakup occurs when the drop passes a critical Weber number. Values for this critical Weber number vary widely in the literature.

The Weber number is given by:

$$We_p = \frac{\rho_a V^2 d}{\sigma}$$

For water drops falling at their terminal velocity, the critical Weber number (based on air density) is approximately 10. For water drops accelerated by a shock wave, a value of 6.5 is given. As drops accelerate toward the airfoil, the lower number appears to be more applicable. The Weber number of each trajectory was output from LEWICE 1.6 for the case described above to investigate this effect. A contour plot of Weber number is shown in Figure 2 and shows that the Weber number clearly indicates that drop breakup occurs for this drop size.

FIGURE 2. Weber number on 1000 micron drop



Drop breakup is also attributed to the Eötvös number, which is given by

$$Eo_p = \frac{a_p \rho_p d^2}{\sigma}$$

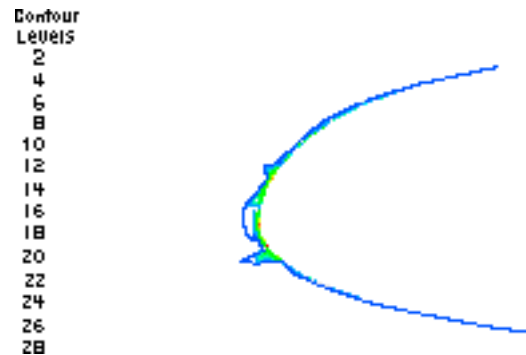
where

$$a_p = \sqrt{\dot{x}^2 + \dot{y}^2}$$

is the acceleration of the particle.

A critical Eötvös value of 16 or higher is cited for drop breakup. The corresponding plot of Eötvös number is shown in Figure 3. This shows that although the Weber number is high enough to cause breakup, Eötvös number is not.

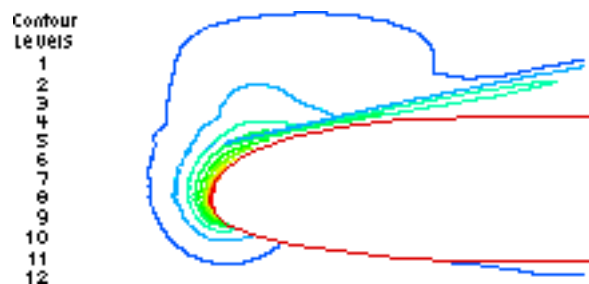
FIGURE 3. Eötvös number on 1000 micron drop



The case for a 1000 μm drop clearly shows that according to the Weber number criteria, drops will breakup before reaching the airfoil. At this point, it is unclear how this breakup effects the collection efficiency. The smaller drops produced will tend to be deflected more, however by the time they reach critical Weber number values, they are only 0.1 chord from the leading edge even in this extreme example. As most of the particle deflection occurs within this region and since drops tend to break up into much smaller drops, it seems feasible that there is some mass loss which can be attributed to this factor.

Figure 2 can be compared to Fig. 4, which shows the Weber number on the drop at 100 microns instead. In this case, the Weber number is at the threshold of droplet breakup. The distortions in the contour plots are caused by the manner in which the plots were produced. The trajectory points were input into PLOT3D as a 'grid'. However, since the time stepping on each trajectory is different, the 'grid' points do not align well, causing the distortions.

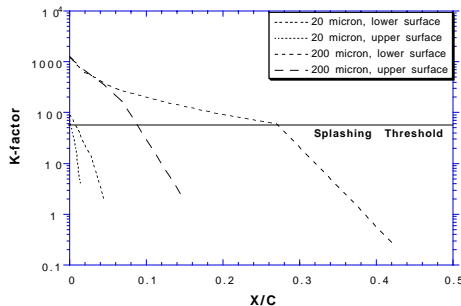
FIGURE 4. Weber number on 100 micron drop



Drop Splashing

LEWICE 1.6 assumes that all drops which strike the surface impinge, thus neglecting splashing and/or bouncing of drops. A recent experimental study by Mundo, Sommerfeld and Tropea⁷ categorizes droplet-wall collisions and correlates splashing in terms of Reynolds number and Ohnesorge number ($Oh = \sqrt{We}/Re = \mu/\sqrt{(\rho\sigma d)}$). These numbers are based on the liquid properties and the component of the impact velocity normal to the surface. Based on the results of their experiment, splashing occurs if the factor $K = Oh * Re^{1.25}$ is greater than 57.7. A plot of this parameter for drop sizes of 20 and 200 microns is shown in Figure 5.

FIGURE 5. K-factor for droplet splash



A small amount of droplet splash is seen in Fig. 5 even for a 20 micron drop, showing that this phenomena will occur at much lower drop sizes than droplet breakup. This figure also shows that droplet splashing is a significant factor in the large drop regime. The Mundo paper also provides a characterization of the size, velocity and direction of the splashed particles. By knowing these parameters, a feature can be added to LEWICE 1.6 to track the trajectories of the splashed particles and the trajectories of particles after breakup. As this modification has not yet been made, a more qualitative approach is taken by analyzing the current trends as drop size increases. This approach will now be presented.

Parameter Study

The capabilities of LEWICE 1.6 in the large drop regime were evaluated by means of a parameter

study on drop size. Twenty cases were performed using drop sizes ranging from 10 microns to 1000 microns. The airfoil used for these runs was a 3 foot chord MS-317 airfoil. This model was chosen as it is available for testing in the IRT. It is therefore possible to verify these results with a future IRT test. The meteorological conditions ran were:

- $\alpha = 2^\circ$
- LWC = 0.34 g/m³
- V = 195 mph
- T = -10 °C
- MVD = 10 μm to 1000 μm

Figures 6-8 show the collection efficiency of each drop size ran in this study. The maximum local collection efficiency increases with drop size, both the upper and lower limits are further downstream with drop size and the total collection efficiency increases with drop size. All of these trends are expected and intuitive. Figure 6 shows a large variation over the initial drop size range while in Fig. 7 this trend slows somewhat and finally, collection efficiency is nearly the same for the very large drop size range. This occurs because the larger drops have so much inertia that their trajectory is nearly ballistic.

FIGURE 6. Collection efficiencies for MVD from 10 to 80.

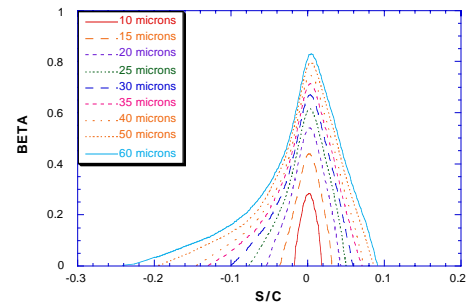


FIGURE 7. Collection efficiency for MVD from 80 to 300

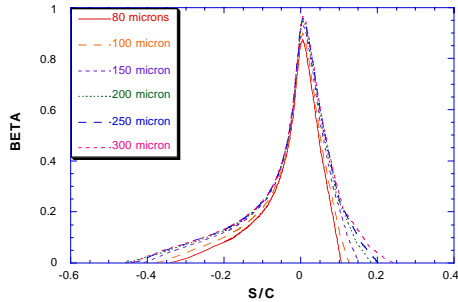
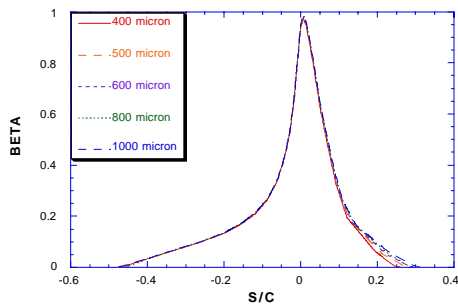


FIGURE 8. Collection efficiency for MVD from 400 to 1000.



Since this analysis focuses on the major characteristics, maximum collection efficiency, impingement limit and total collection efficiency, these parameters are also plotted in Figs. 9-11.

FIGURE 9. Maximum beta as a function of drop size.

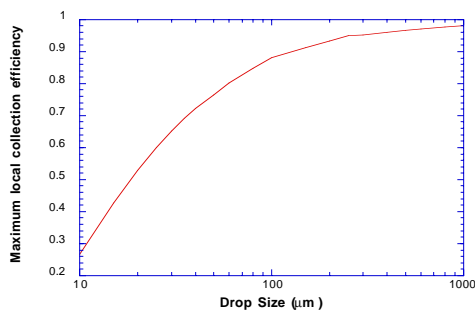


FIGURE 10. Impingement limit as a function of drop size.

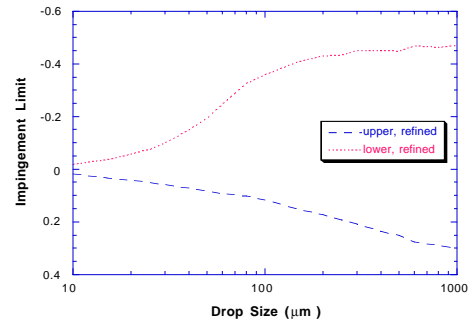
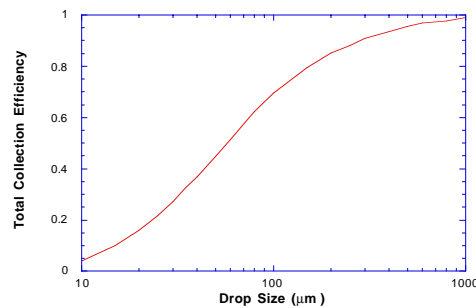


FIGURE 11. Total collection efficiency as a function of drop size.



These plots reveal the reasons why there is an upper limit to the local collection efficiencies shown earlier. The larger a drop gets, the more ballistic its trajectory will be and the local collection efficiency is simply a reflection of the curvature of the airfoil geometry.

Figure 9 shows the maximum local collection efficiency. Since this cannot, by definition, be greater than one for an MS-317 airfoil, this provides one limitation with drop size. Figure 10 shows the upper and lower impingement limits. The theoretical limit are the maximum and minimum thickness of the airfoil. At a 2° angle of attack, these are at approximately $x/c=0.3$ and $x/c=0.45$ respectively. The 1000 μm drop size impingement limit is very close to this value.

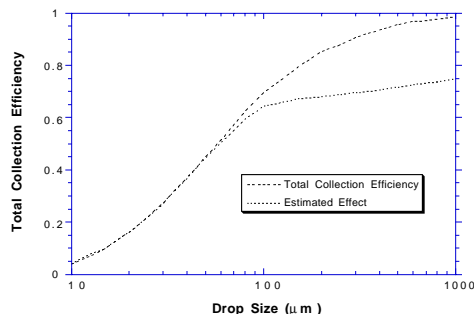
The theoretical limitations are best shown in Figure 11. The total collection efficiency is the integral of the local values normalized to the airfoil thickness.

This shows the degree to which the drops are deflected by the airfoil. If the drops come in with no deflection, the total collection efficiency is one. This curve shows a rapid increase in total collection efficiency up to 100-200 micron range, then a tapering off to nearly 1 at 1000 microns.

A prediction of the change in results once droplet breakup and droplet splash are considered can now be estimated. Both of these factors will result in a loss of mass, especially at the stagnation point where the Weber numbers are shown to be the highest. This mass loss will result in a lower maximum collection efficiency and lower total collection efficiencies. Less of an effect will be seen at the impingement limits where the Weber number is lower. Since the limiting total collection efficiency will be lower, this limiting value will be reached at a smaller drop size. Since the larger drops are breaking up and splashing into smaller drops, this also established a lower theoretical limit.

Figure 12 shows an estimate where this lower limit is established closer to 100 microns instead of 1000. The limit was placed at this level because there is no drop breakup at this drop size and splashing is limited to the leading edge. LEWICE 1.6 (as well as other codes) will overpredict results by 20-30% at a 1000 μm drop and approximately 10% at 100 μm based on this analysis.

FIGURE 12. Estimated effect of Splashing



Multi-Element Ice Accretion

As described in an earlier report¹, LEWICE 1.6 has the capability to predict ice shapes on multi-element configurations. Often, the limitations of potential

flow make these predictions much less accurate than more sophisticated flow models, but it may be adequate for the purpose of providing sample ice shapes. The multi-element trajectory, ice accretion and ice growth models will be converted for use with more accurate flow solvers.

LEWICE 1.6 performs multi-element trajectories by treating each element as a single entity. Impingement limits and collection efficiencies are determined on each body as though the other bodies are not there. Their influence on the trajectories is embedded in the flow solution, which takes into account all of the bodies. Any trajectory hits on other elements are treated as missed trajectories.

The hits on other bodies are, however, useful in determining the starting location of the next trajectory in the impingement limit search, especially hits on bodies which precede the one selected. For example, when the code looks for impingement limits on the flap(s), trajectory hits on the slat are useful in determining the starting location of the next trajectory. Routine MODE in LEWICE 1.6 determines if a trajectory hits or misses a body. It was modified so that it not only knew that a body was hit, but which one. As stated earlier, hits on other bodies are only used to select the starting location of the next trajectory.

An additional problem occurs especially on the main element of a multi-element airfoil. It is possible for trajectories to hit this element by passing above the slat as well as by passing below the slat. Therefore, for all bodies but the first one (the slat) LEWICE 1.6 will first look below the slat for an upper and lower impingement limit and determine one set of collection efficiencies for this set of impingement limits. LEWICE 1.6 will then look above the slat and attempt to find a second set of impingement limits. If two sets of limits are found, the two collection efficiency arrays are merged.

The process of converting LEWICE to handle multi-element geometries was made more difficult by the addition of the multiple geometry scheme used to increase the accuracy of the code. After the trajectory routine is completed, LEWICE creates a second set of panels for each element and resolves the flow field using this panel set. For a single element case, this second set of panels produces a smoother pressure distribution which increases the accuracy of the boundary layer integration. This is not always the case for multiple element geometries. Work is con-

tinuing on this routine so that this very useful feature is better integrated with multi-element geometries.

Once the collection efficiencies for each element has been found, and the flow recalculated, LEWICE 1.6 is ready to perform the boundary layer integration and the ice accretion. Once again, this procedure is performed on each element individually, without regard to the presence or influence of other elements. The geometry modification is performed on each element individually, hence the code does not currently check for different elements intersecting due to ice growth. In this case, the code will most likely crash when it tries to solve the flow field on the next time step.

The example case used to illustrate the multi-element capabilities shows a comparison between this code and experimental data taken on a 3-element McDonnell-Douglas airfoil. The airfoil is shown in Figure 13. The experimental data is documented in another paper at this conference⁴. The conditions for the comparison were:

landing configuration (30° flap)
 $V = 198$ mph
 $T = -5$ °C
 $LWC = 0.6$ g/m³
 $MVD = 20$ μm
 8° angle of attack
 time = 6 minutes

The ice shape comparisons are shown in Figs. 14-16. Due to the complex geometry, a Langmuir 'D' droplet distribution consisting of 7 drop sizes was used in the numerical prediction. The prediction on the slat is quite good, which can be expected as the flow situation is similar to that for a single element airfoil. The upper horn angle is slightly off and the lower shape is very slightly less, but the general shape and impingement limits are well predicted.

The ice shape on the main element and flap is under predicted, although LEWICE 1.6 captures the shape on the leading edge of the flap. In the experiment, both the main body and flap have ice growth over much of the lower surface.

FIGURE 13. McDonnell-Douglas airfoil

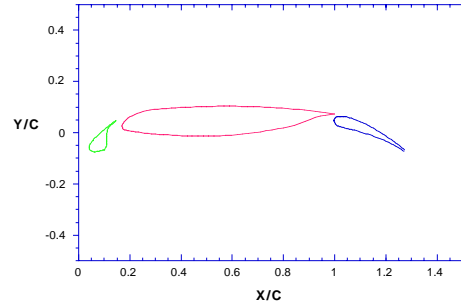


FIGURE 14. Slat ice shape comparison

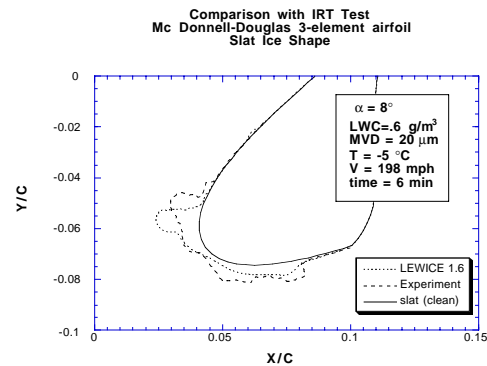


FIGURE 15. Main ice shape comparison

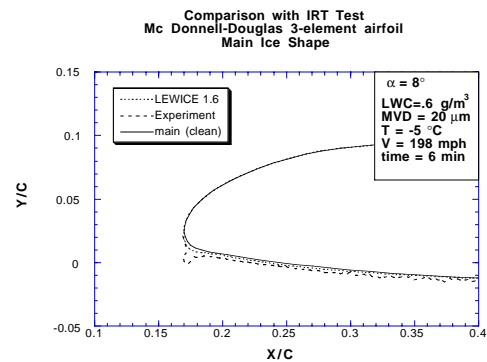
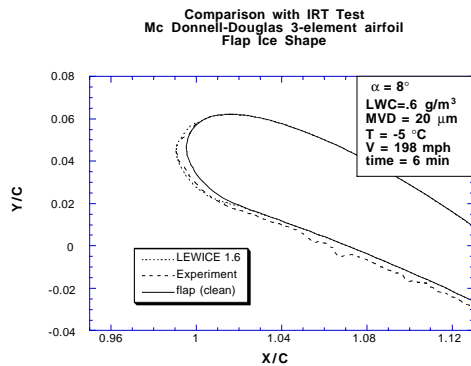
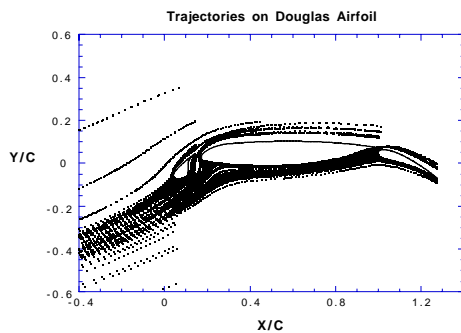


FIGURE 16. Flap ice shape comparison



The likely cases of this discrepancy are: tunnel turbulence, which causes more water to impinge than would actually occur in flight; the inadequacy of potential flow to correctly model the flow on the aft bodies; or there could be a problem with the code, as this feature is still very new. The difference is not as great as it may otherwise seem if one looks at Fig. 16, which is a plot of the droplet trajectories on the clean airfoil. This figure shows that the drops are travelling very close to both the main body and the flap without impinging. Even a small upward change in the flow would cause an increase in the number of drops which impinge and provide a better comparison. Future work in this area is aimed at interfacing the multi-body trajectory portion of LEWICE 1.6 with higher level flow solvers so that these questions may be answered.

FIGURE 17. Drop trajectories on Douglas airfoil



'Blind' Test

A 'blind' test is defined as a case where a code predicts the outcome without knowing the experimental results beforehand. It is useful so that others may make an objective evaluation of how far the development effort has progressed. This is the first known 'blind' test of an ice accretion code. Prior to this, code developers could adjust parameters such as 'sand-grain' roughness, time step and other variables to improve the prediction. Then only the best comparisons are presented.

This section will present the predicted ice shapes for a GLC305 Learjet airfoil which is scheduled for testing in the IRT in late July/early August 1995. The test points represent points on the continuous max of the FAA Appendix C icing envelope or the closest point based on tunnel limitations. Cases 7-9, 26, 27, 32 and 33 differ from the continuous max conditions because of tunnel limitations. Cases 36-39 represent the closest points to the intermittent max that the tunnel will run. As this paper was completed before the start of the test, no comparisons can be made with the data. The following plots contain the LEWICE 1.6 predictions for every condition which is in the planned test matrix.

FIGURE 18. LEWICE 1.6 prediction for cases 1-3.

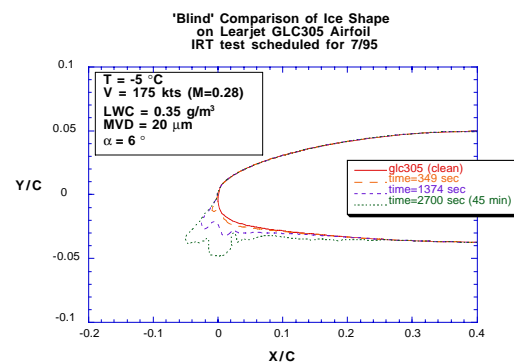


FIGURE 19. LEWICE 1.6 prediction for cases 4-6.

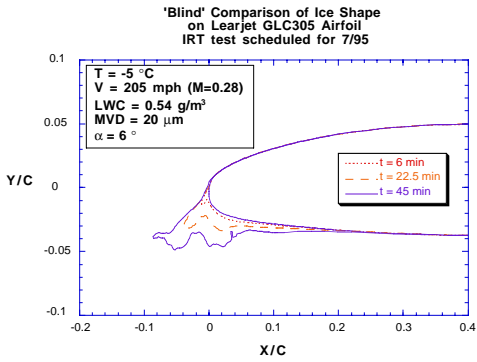


FIGURE 20. LEWICE 1.6 prediction for cases 7-9.

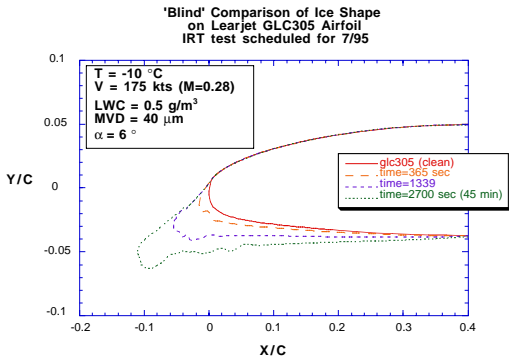


FIGURE 21. LEWICE 1.6 prediction for cases 10-12.

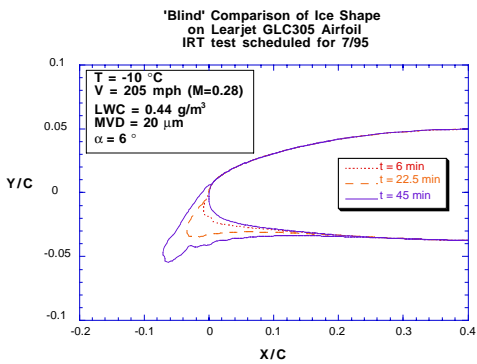


FIGURE 22. LEWICE 1.6 prediction for cases 13-15.

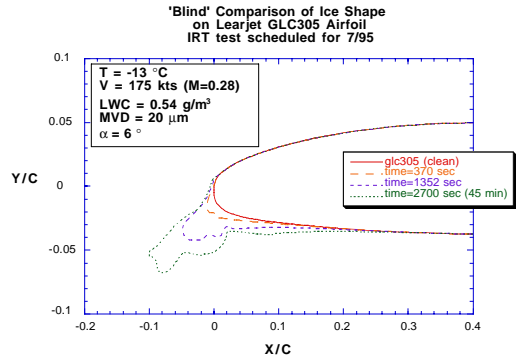


FIGURE 23. LEWICE 1.6 prediction for cases 16-18.

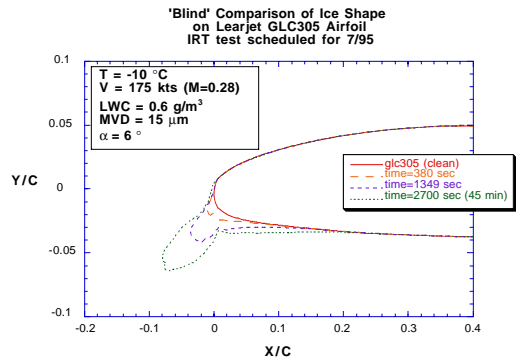


FIGURE 24. LEWICE 1.6 prediction for cases 19-21.

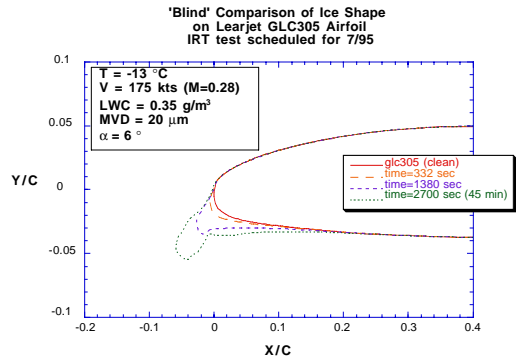


FIGURE 25. LEWICE 1.6 prediction for cases 22-23.

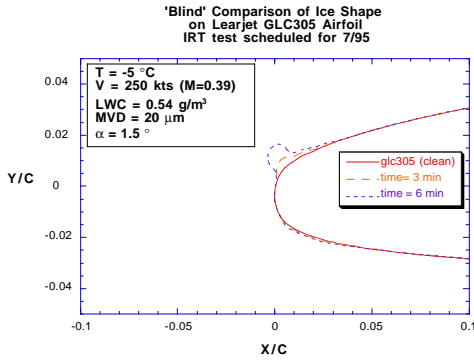


FIGURE 26. LEWICE 1.6 prediction for cases 24-25.

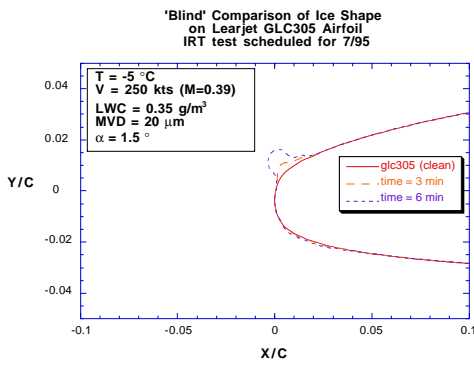


FIGURE 27. LEWICE 1.6 prediction for cases 26-27.

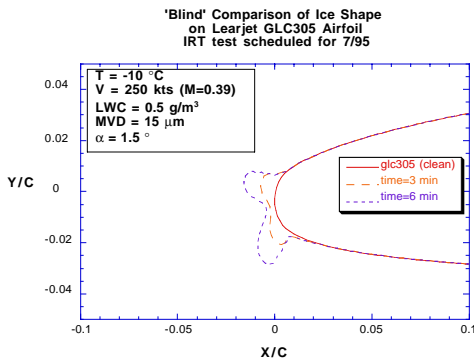


FIGURE 28. LEWICE 1.6 prediction for cases 28-29.

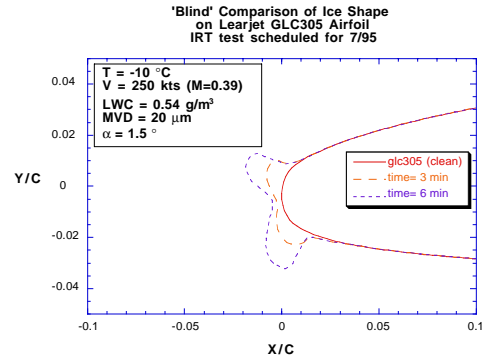


FIGURE 29. LEWICE 1.6 prediction for cases 30-31.

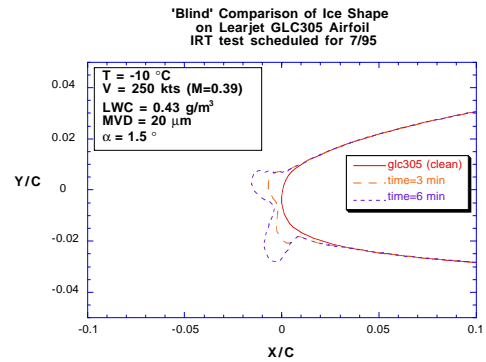


FIGURE 30. LEWICE 1.6 prediction for cases 32-33.

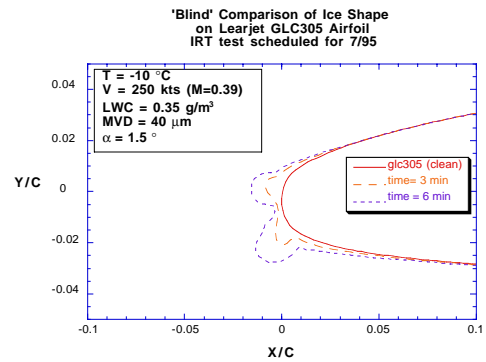


FIGURE 31. LEWICE 1.6 prediction for cases 34-35.

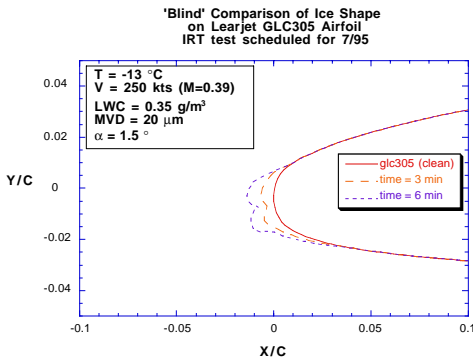


FIGURE 32. LEWICE 1.6 prediction for case 36.

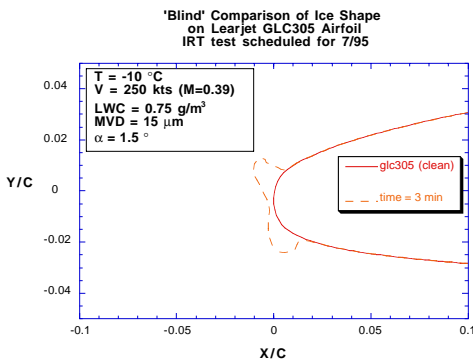


FIGURE 33. LEWICE 1.6 prediction for case 37.

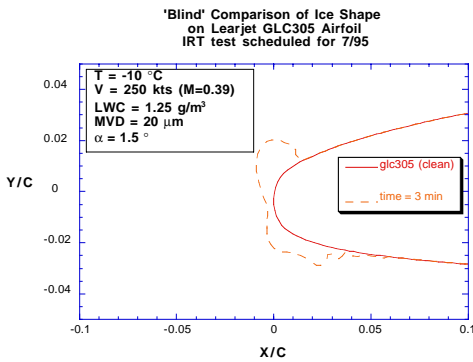


FIGURE 34. LEWICE 1.6 prediction for case 38.

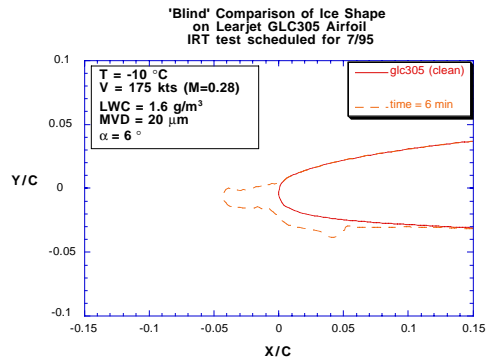
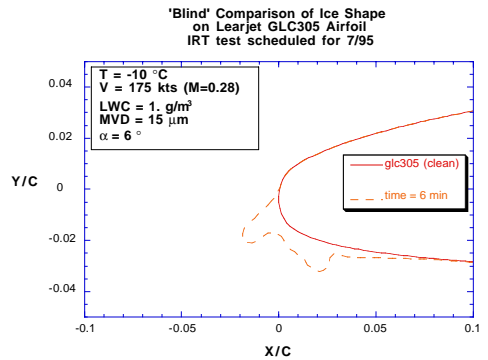


FIGURE 35. LEWICE 1.6 prediction for case 39.



Conclusions

Three features of LEWICE 1.6 have been presented in this paper. First, the droplet trajectory equations were examined for their applicability in the large drop regime. A parameter study was performed to estimate the mass loss due to droplet breakup and droplet splash, which are the major changes which will occur in this regime. For the example cited, it is estimated that 10% mass loss occurs around 100 microns up to 20-30% mass loss around 1000 microns, resulting in a condition where the collection efficiency changes only slightly over this region. Using LEWICE 1.6 as it stands now will result in a conservative prediction of water loading and impingement limits. The user is cautioned that these estimates depend not only on drop size, but on velocity as well. The key parameter is the Weber number,

which is proportional to drop size but is proportional to velocity squared. Therefore, velocity will play a large factor in the determination of the upper limit to the total collection efficiency.

Second, the capabilities of LEWICE 1.6 for multi-element ice accretion were demonstrated with a comparison with experimental ice shape data taken on a McDonnell-Douglas 3-element high-lift airfoil. The comparisons were very good, although LEWICE 1.6 underpredicted the extent of ice on the main body and flap. This discrepancy could be due to several factors, including tunnel effects. The comparison on multi-element airfoils is much improved over that shown in an earlier report¹. Several improvements were made to the code in the interim. In addition, the Boeing data set was compared at several locations to show that there were problems in that test with uniformity, indicating spanwise effects.

Third, 39 predictions were shown for a Learjet GLC305 airfoil for which the experimental data will be taken later in the year. By publishing the data before the experiment, this marks the first 'blind' test of an ice accretion code. In addition, predictions for the entire test matrix were provided to provide an objective evaluation of the code for a large variety of conditions. A second paper is planned which will provide details of the test and comparison with these results.

In conclusion, LEWICE 1.6 has been shown to be a very robust code for predicting droplet trajectories and ice accretion for numerous different conditions. Research is continuing on improving the physical models within the code in order to produce a code which can accurately predict ice shapes for any condition.

References

1) Wright, W. B. and Bidwell, C. S., "Additional Improvements to the NASA Lewis Ice Accretion Code LEWICE," NASA TM (AIAA-95-0752), Jan. 1995.

3) Wright, W.B., "Users Manual for the Improved NASA Lewis Ice Accretion Code LEWICE 1.6," NASA CR198355, June 1995.

3) Wright, W.B., Bidwell, C. S., Potapczuk, M. G. and Britton, R. K. "Proceedings of the LEWICE Workshop," June 1995 (to be published).

4) Khodadoust, A., Dominik, C., Shin, J. and Miller, D. "Effect of In-Flight Ice Accretion on the Performance of a Multi-Element Airfoil," presented at the SAE/AHS International Icing Symposium, Sept. 1995.

5) Clift, R., Grace, J. R., and Weber, M. E., "Bubbles, Drops, and Particles," Academic Press, New York, 1978.

6) Beard, K. V., and Pruppacher, H. R., "A Determination of the Terminal Velocity and Drag of Small Water Drops by Means of a Wind Tunnel," J. Atmos. Sci, v. 26, pp. 1066-1072, 1969.

7) Mundo, C., Sommerfeld, M., and Tropea, C., "Droplet-Wall Collisions: Experimental Studies of the Deformation and Breakup Process," Int. J. Multiphase Flow, v. 21, No. 2, pp. 151-173, 1995.